Dalton Transactions

PAPER

View Article Online
View Journal | View Issue



Cite this: *Dalton Trans.*, 2014, **43**, 1424

# Electron transfer and binding affinities in an electrochemically controlled ligand transfer system containing zinc porphyrin and a *meso*-phenylenediamine substituent†

Hsu Chun Cheng,[a] Peter Ping Yu Chen*[b] and Yuhlong Oliver Su*[a]

Received 6th September 2013,
Accepted 24th October 2013

DOI: 10.1039/c3dt52463a

www.rsc.org/dalton

Investigations on the transfer of the ligand, imidazole (HIm), between two covalently linked redox centres – zinc porphyrin and phenylenediamine (**PD**) – and the influence of the length of the linker are reported. Since the binding affinity of the ligand with zinc porphyrin is different from that of the ligand with the phenylenediamine moiety, the transfer of the ligand could be electrochemically controlled by adjusting the oxidation potentials. Changes in cyclic voltammograms and absorption spectra of the complexes revealed the site of ligand binding in the various oxidation states of the modified zinc porphyrins. Binding constants of the modified zinc porphyrins in various oxidation states were also determined by photometric titration with the ligand and digital simulations. Evidence for the delocalization of the electron from the zinc porphyrin to the phenylenediamine moiety and the influence of the delocalization on them were obtained from EPR studies.

## Introduction

Porphyrins and metalloporphyrins have widespread applications in catalysis,[1,2] electron-transfer systems[3–8] and photoelectric devices.[5–8] For the biological process involving metalloporphyrins, the respiratory process occurs in the mitochondria resulting in the formation of adenosine triphosphate, while haemoglobin and myoglobin act as dioxygen carriers. These critical processes are popular areas of research.[9–11] These systems involve multiple redox centres. On the other hand, imidazole the functional side chain of histidine in enzymes and proteins acts as a ligand in several metalloproteins and influences their behaviour.[9–11] Furthermore, the properties of a redox centre can be influenced by the proximity of a second redox centre. Therefore, the properties related to redox dependent ligation of a ligand and intramolecular electron transfer in a system with multiple redox centres and multiple sites of ligation should be further examined and clarified. Our group has recently reported on an imidazole (HIm) shuttling system **ZnTMP-PD** consisting of a zinc porphyrin (**ZnTMP**) covalently linked to a phenylenediamine (**PD**).[12] The ligation of HIm to the zinc porphyrin centre was indicated in the neutral state. When the **ZnTMP-PD** was partially oxidized (−2e), the electron deficient **PD** became the binding site for HIm. Since the reported formation constant ($K$) of oxidized species with a ligand is $\sim 10^5$ $M^{-1}$,[13–15] we proposed that upon further oxidation of **ZnTMP-PD**, HIm would likely revert back to the zinc porphyrin moiety because the formation constant between the cation radical of zinc porphyrin and the ligand is $\sim 10^7$ $M^{-1}$.

We have now revisited the system containing zinc porphyrin and phenylenediamine linked to each other *via* a covalent bridge to determine the binding constant of HIm with each moiety at various oxidation states and to study the influence of the covalent bridge (the distance between **ZnTMP** and **PD**) on this phenomenon. The use of phenyl groups is a straightforward and basic way to separate two redox centres. The interaction between one redox centre to another could be considered as that of an electron-donating or -withdrawing group based on the change in the electron cloud distribution after an electrochemical procedure. We have now synthesized a series of zinc porphyrins, in which the bridge length is elongated by phenyl groups (Chart 1). Binding affinities were determined by photometric titrations and evaluated by digital simulations. The ligand transfer behaviour was monitored by cyclic voltammograms (CVs) and optically transparent thin-layer electrode (OTTLE) spectroelectrochemical methods. Furthermore, details of the electron delocalization in these

[a]*Department of Applied Chemistry, National Chi Nan University, 1, University Road, Puli, Nantou, 545, Taiwan. E-mail: yosu@ncnu.edu.tw; Fax: (+886)49-2917956*
[b]*Department of Chemistry, National Chung Hsing University, 250, Kuo Kuang Road, Taichung, 402, Taiwan. E-mail: pychen@dragon.nchu.edu.tw; Fax: (+886)4-22840411*

†Electronic supplementary information (ESI) available: $^1$H NMR, $^{13}$C NMR spectra, and electrochemical analysis. See DOI: 10.1039/c3dt52463a

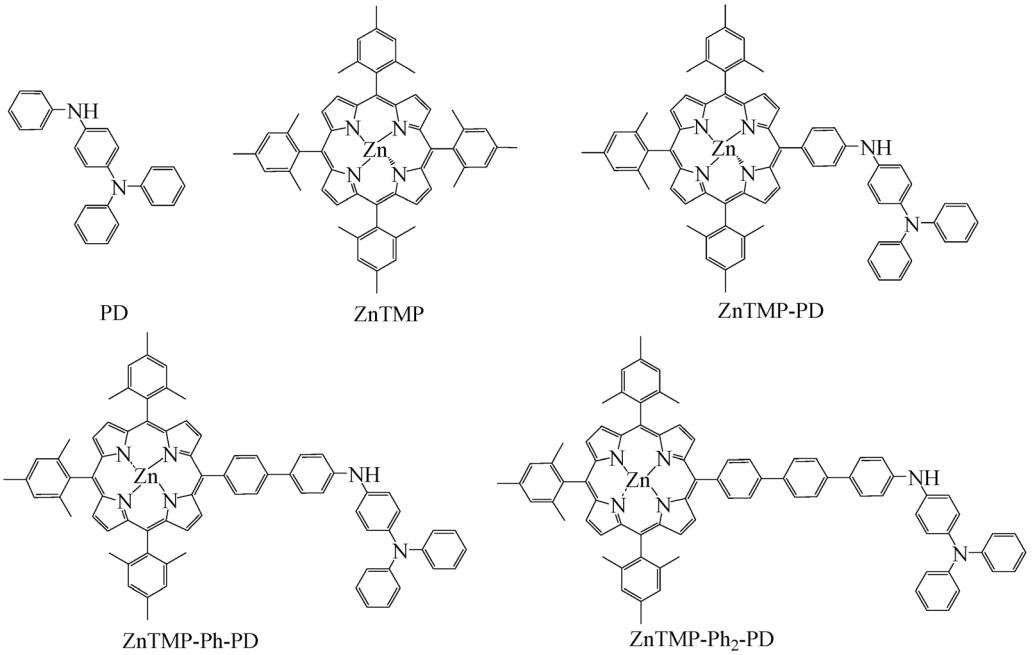


**Chart 1** Structures of phenylenediamine (**PD**) and **PD**-substituted zinc porphyrins.

systems were obtained by electron paramagnetic resonance (EPR) studies.

## Experimental section

Chemicals for synthesis were obtained commercially from ACROS (Geel, Belgium). Organic solvents were dried before use. Analytical grade tetra-*n*-butylammonium perchlorate (TBAP) for use in electrochemical experiments was also obtained from ACROS (Geel, Belgium) and recrystallized twice from ethyl acetate and then dried in a vacuum prior to use.

Electrochemistry was performed using a CHI Model 760 series electroanalytical workstation (CH Instruments, Inc., Texas, USA). Cyclic voltammetry was conducted with the use of a three-electrode cell in which a BAS glassy carbon electrode (area = 0.07 $cm^2$) was used as the working electrode. The glassy carbon electrode was polished with 0.05 μm alumina on Buehler felt pads and was sonicated for 2 min in an ultrasound bath to remove the alumina residue. The platinum wire served as an auxiliary electrode and the reference electrode was a home-made Ag/AgCl, KCl(sat'd) reference electrode. The spectroelectrochemical cell was composed of a 1 mm cuvette, a thin layer carbon gauze as a working electrode, a platinum wire as an auxiliary electrode, and an Ag/AgCl, KCl(sat'd) reference electrode. The environment of cyclic voltammetry and spectroelectrochemical experiment is $CH_2Cl_2$ containing the supporting electrolyte, tetrabutylammonium perchloride (TBAP). The recorded CV was simulated by DigiSim (v 3.03, Bioanalytical Systems, Inc., West Lafayette, IN, USA). Absorption spectra were measured using a HP-8453 UV-Vis spectrophotometer (Agilent Technologies, Santa Clara, CA, USA). $^1$H NMR and $^{13}$C NMR spectra were obtained using a Varian Unity Inova 300 WB spectrometer (Varian Assoc., Palo Alto, CA, USA). EPR spectra were obtained using a Bruker Model EMX-10/12 spectrometer (Bruker Optic GmbH, Karlsruhe, Germany).

### Synthesis

Compounds **1**, **3**, and **4** were synthesized in 53%, 50% and 73% yields, respectively, following methods reported in the literature.[12,16]

**4′-Bromo-4-triphenylbenzaldehyde (2).** A catalytic amount (3%–5% mol) of tetrakis-triphenylphosphine palladium and 3.0 mL of aqueous 2 M $Na_2CO_3$ were added to a solution of 4-bromo-4′-iodobiphenyl (2.39 g, 6.67 mmol) in 20 mL of toluene. A solution of 4-formylbenzeneboronic acid (1.00 g, 6.67 mmol) in 20 mL of ethanol was subsequently added, and the mixture was heated to reflux for 3 hours in an argon atmosphere. After cooling, the mixture was extracted with dichloromethane (three times) and the combined organic phase was washed with water and brine, dried, and evaporated under vacuum. The residue was purified by chromatography to give **2** in 50% yield (1.12 g, white solid). $^1$H NMR (300 MHz, $CD_2Cl_2$) $\delta$(ppm) = 7.58 (4H, q), 7.74 (4H, q), 7.83 (2H, d), 7.97 (2H, d) and 10.06 (1H, s); $^{13}$C NMR (75 MHz, $CDCl_3$) $\delta$(ppm) = 127.5, 127.8, 128.1, 128.2, 128.4, 129.0, 129.2, 129.4, 129.5, 130.6, 132.5, 135.9, 140.3, 148.6. Anal. Calc. for $C_{19}H_{13}BrO$: C 67.67; H 3.89%; found: C 67.52; H 3.95% (Fig. S11 and S12, ESI†).[16]

**Zn(Ph$_2$-Br)(mesityl)$_3$P (5).** Pyrrole (0.67 mL, 10.0 mmol), 4′-bromobiphenyl-4-carbaldehyde (0.65 g, 2.5 mmol), and mesitylaldehyde (1.34 g, 10.0 mmol) were mixed in 1000 mL $CHCl_3$ under a nitrogen atmosphere for 10 min. $BF_3{\cdot}OEt_2$ (0.85 mL, 6.77 mmol) was added to this mixture. After stirring for about an hour, 2,3-dichloro-5,6-dicyanobenzoquinone (DDQ, 1.75 g,

7.55 mmol) was added for 1 hour. Finally, triethylamine (0.46 mL, 3.30 mmol) was added for 30 min. The resulting precipitate was filtered and washed with methanol, dissolved in a minimum quantity of dichloromethane, and chromatographed on silica gel (eluting with a solution of dichloromethane) to afford a purple solid. This solid was a mixture of compounds that were difficult to separate over a column of silica. We inserted zinc into the porphyrin product to enhance the polarity difference between the desired product and other by-products and thereby assist in its purification. Complexation with zinc was performed by mixing a solution of crude products in $CH_2Cl_2$ with zinc acetate (1.0 g, 5.45 mmol) in MeOH for 3 hours, and the solution was monitored by UV-Vis spectroscopy till the initial spectrum had completely changed. The solution was extracted with water (3 times) and the concentrated organic layer was purified by chromatography over silica gel in which the elution solution was dichloromethane–hexane = 1 : 5 to afford **5** in 6.3% yield (152 mg, red-purple solid); $^1$H NMR (300 MHz, $CD_2Cl_2$) $\delta$(ppm) = 1.84 (18H, s), 2.62 (9H, s), 7.29 (6H, s), 7.72 (2H, d), 7.83 (2H, d), 7.97 (2H, d), 8.31 (2H, d), 8.71 (4H, s), 8.76 (2H, d), and 8.94 (2H, d); $^{13}$C NMR (75 MHz, $CDCl_3$) $\delta$(ppm) = 21.9, 118.9, 119.1, 119.6, 122.0, 125.2, 127.8, 129.2, 130.9, 131.3, 132.3, 132.3, 135.2, 137.6, 139.0, 139.2, 139.3, 139.5, 139.7, 140.1, 142.7, 149.9, 150.0, 150.1. Anal. Calc. for $C_{59}H_{49}BrN_4Zn$: C 73.87; H 5.15; N 5.84%; found: C 74.12; H 5.23; N 5.88% (Fig. S13 and S14, ESI†).

**Zn(Ph$_3$-Br)(mesityl)$_3$P (6).** Pyrrole (0.67 mL, 10.0 mmol), 4′-bromo-4-triphenylbenzaldehyde (0.65 g, 2.5 mmol), and mesitylaldehyde (1.34 g, 10.0 mmol) were mixed in 1000 mL $CHCl_3$ solution under a nitrogen atmosphere for 10 min. $BF_3{\cdot}OEt_2$ (0.85 mL, 6.77 mmol) was then added to this mixture. After stirring for about an hour, 2,3-dichloro-5,6-dicyanobenzoquinone (DDQ, 1.75 g, 7.55 mmol) was added for 1 hour. Finally, triethylamine (0.46 mL, 3.30 mmol) was added for 30 min. The resulting precipitate was filtered and washed with methanol, taken into a minimum of dichloromethane, and chromatographed on silica gel (eluting with a solution of dichloromethane) to afford a purple solid which was a mixture of products and other compounds. Complexation with zinc and subsequent purification over silica gel conducted in accordance with the procedure described in the purification of compound **5** gave **6** in 7% yield (192 mg, red-purple solid); $^1$H NMR (300 MHz, $CD_2Cl_2$) $\delta$(ppm) = 1.86 (18H, s), 2.62 (9H, s), 7.30 (6H, s), 7.62 (2H, s), 7.78 (2H, d), 8.01 (4H, t), 8.33 (2H, d), 8.73 (4H, s), 8.78 (2H, d), and 8.99 (2H, d); $^{13}$C NMR (75 MHz, $CDCl_3$) $\delta$(ppm) = 21.9, 118.8, 119.1, 119.8, 119.9, 121.9, 125.3, 127.3, 127.7, 127.9, 128.0, 128.9, 129.1, 129.2, 130.9, 131.4, 132.2, 132.3, 135.2, 137.6, 139.3, 139.5, 139.8, 140.5, 142.5, 149.9, 150.1. Anal. Calc. for $C_{65}H_{53}BrN_4Zn$: C 75.40; H 5.16; N 5.41%; found: C 75.28; H 5.26; N 5.34% (Fig. S15 and S16, ESI†).

**ZnTMP-Ph-PD.** A 30 mL toluene solution of compound **5** (80.00 mg, 0.083 mmol) and *t*-BuONa (26.45 mg, 0.275 mmol) and another 30 mL toluene solution containing TPA-$NH_2$ (65.13 mg, 0.250 mmol), $Pd(OAc)_2$ (3.82 mg, 0.004 mmol), and dppf (2.31 mg, 0.004 mmol) were stirred separately at room temperature for 15 min. The two solutions were mixed and refluxed at 110–115 °C for 48 hours under a nitrogen atmosphere. The reaction solution was filtered and then chromatographed on silica gel (eluting with a solution of dichloromethane–hexane = 1 : 3) to afford **ZnTMP-Ph-PD** in 48% yield (45 mg, purple solid); $^1$H NMR (300 MHz, $CD_2Cl_2$) $\delta$ (ppm) = 1.84 (18H, s), 2.62 (9H, s), 5.98 (1H, s), 6.98 (2H, t), 7.15 (2H, d), 7.23 (12H, q), 7.84 (2H, d), 7.97 (2H, d), 8.27 (2H, d), 8.70 (4H, s), 8.75 (2H, d), and 8.97 (2H, d) (Fig. S10†); $^{13}$C NMR (75 MHz, $CDCl_3$) $\delta$(ppm) = 21.9, 117.5, 118.0, 118.7, 119.0, 120.0, 120.2, 122.3, 127.9, 128.4, 129.4, 130.8, 131.3, 132.4, 133.2, 135.1, 137.6, 138.7, 139.2, 139.3, 139.5, 139.8, 141.4, 143.4, 148.3, 149.9. Anal. Calc. for $C_{77}H_{64}N_6Zn$: C 81.21; H 5.66; N 7.38%; found: C 81.36; H 5.71; N 7.32%. HRMS calcd for $[C_{77}H_{65}N_6Zn]^+$ = 1136.4512, found: 1136.4533 (Fig. S17 and S18, ESI†).

**ZnTMP-Ph$_2$-PD.** A 30 mL toluene solution of compound **6** (50.00 mg, 0.048 mmol) and *t*-BuONa (23.20 mg, 0.241 mmol) and another 30 mL toluene solution containing TPA-$NH_2$ (62.87 mg, 0.242 mmol), $Pd(OAc)_2$ (3.82 mg, 0.004 mmol), and dppf (2.31 mg, 0.004 mmol) were stirred separately at room temperature for 15 min. Under a nitrogen atmosphere, two solutions were mixed and refluxed at 110–115 °C for 48 hours. The reaction solution was filtered, and chromatographed on silica gel (eluting with a solution of dichloromethane–hexane = 1 : 3) to afford **ZnTMP-Ph$_2$-PD** in 41% yield (24 mg, purple solid); $^1$H NMR (300 MHz, $CD_2Cl_2$) $\delta$ (ppm) = 1.84 (18H, s), 2.62 (9H, s), 5.98 (1H, s), 6.98 (2H, t), 7.15 (2H, d), 7.23 (12H, q), 7.84 (2H, d), 7.97 (2H, d), 8.27 (2H, d), 8.70 (4H, s), 8.75 (2H, d), and 8.97 (2H, d) (Fig. S10†); $^{13}$C NMR (75 MHz, $CDCl_3$) $\delta$ (ppm) = 21.9, 117.6, 119.4, 120.3, 121.4, 122.6, 123.7, 125.5, 126.0, 126.2, 127.2, 127.4, 128.2, 128.3, 129.7, 131.1, 131.6, 132.7, 135.5, 138.1, 139.7, 140.1, 140.4, 142.5, 143.9, 148.6, 150.4. Anal. Calc. for $C_{83}H_{68}N_6Zn$: C 82.06; H 5.64; N 6.92%; found: C 82.32; H 5.71; N 6.98%. HRMS calcd $[C_{77}H_{65}N_6Zn]^+$ = 1136.4512, found: 1136.4533 (Fig. S19 and S20, ESI†).

## Results and discussion

### Cyclic voltammograms

To elucidate the electrochemistry of **PD**-substituted zinc porphyrins, the cyclic voltammetry of **PD** and **ZnTMP** were first studied separately. Cyclic voltammograms (CVs) of both **PD** and **ZnTMP** exhibited two well-defined one-electron reversible redox couples. The half potentials ($E_{1/2}$) for **PD** were +0.59 and +1.01 V while those for **ZnTMP** were +0.79 and +1.11 V.[12,17] When **PD** and **ZnTMP** were titrated separately with HIm, their CVs responded differently. In the case of **PD** (Fig. 1(A)), the current of the first redox couple with an $E_{1/2}$ of +0.59 V increased at the cost of the second redox couple, which gradually disappeared. This one-step two electron oxidation is interpreted to result from the electrochemically induced hydrogen bond formation between oxidized **PD** and HIm.[17] Whereas, when **ZnTMP** (Fig. 2) was titrated with HIm, the first redox couple exhibited a cathodic shift (+0.60 V) while the second

 

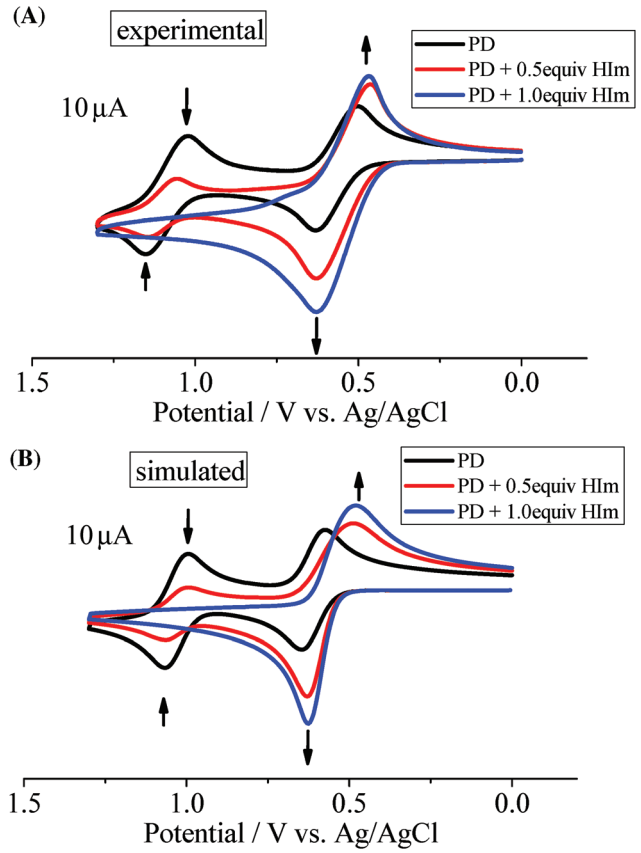


**Fig. 1** (A) Experimental and (B) simulated cyclic voltammetry of 1.0 × $10^{-3}$ M **PD** in $CH_2Cl_2$ containing 0.1 M TBAP in the presence of [HIm] = 0.00–1.00 equiv. Working electrode: glassy carbon. Scan rate: 0.1 V $s^{-1}$.

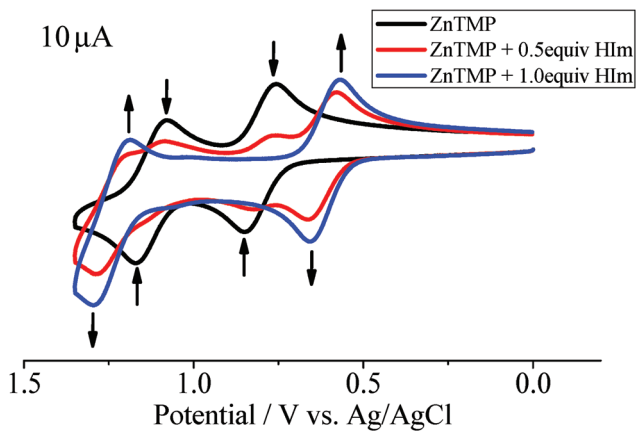


**Fig. 2** Cyclic voltammetry of 1.0 × $10^{-3}$ M ZnTMP in $CH_2Cl_2$ containing 0.1 M TBAP in the presence of [HIm] = 0.00–1.00 equiv. Working electrode: glassy carbon. Scan rate: 0.1 V $s^{-1}$.

redox showed an anodic shift (+1.21 V).[18,19] When the composite molecule **ZnTMP-Ph-PD** (Fig. 3) was scanned, its CV exhibited three redox couples with $E_{1/2}$ of +0.56, +0.82, and +1.12 V. The effect of various concentrations of HIm on $E_{1/2}$ of **ZnTMP-Ph-PD** was investigated. Concurrent with the increase

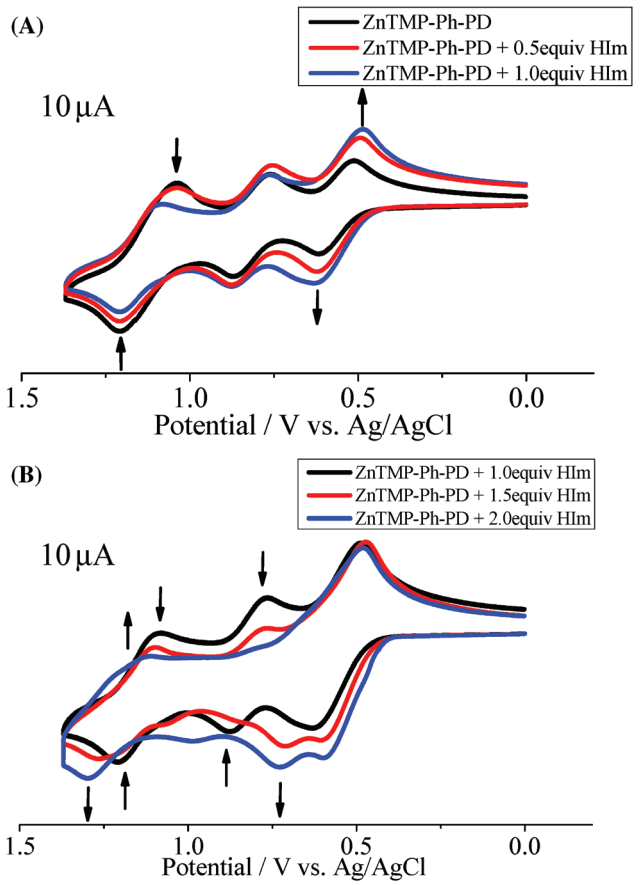


**Fig. 3** Cyclic voltammetry of 1.0 × $10^{-3}$ M **ZnTMP-Ph-PD** in $CH_2Cl_2$ containing 0.1 M TBAP in the presence of (A) [HIm] = 0.00–1.00 equivalent and (B) 1.00–2.00 equivalents. Working electrode: glassy carbon. Scan rate: 0.1 V $s^{-1}$.

in the quantity of HIm to one equivalent of **ZnTMP-Ph-PD**, there was a decrease in the current of the third redox couple and an increase in current of the first redox couple (with $E_{1/2}$ of +0.56, +0.82, and +1.14 V). Further increase in the quantity of ligand to 2.0 equivalents of **ZnTMP-Ph-PD** led to a cathodic shift in the second redox couple and an anodic shift in the third (with $E_{1/2}$ of +0.56, +0.61, and +1.21 V). The results from the voltammetry of **ZnTMP-Ph$_2$-PD** (Fig. S1, ESI†) were similar to those observed for **ZnTMP-Ph-PD**, with the three redox couples at $E_{1/2}$ values of +0.56, +0.80, and +1.10 V. Titration with HIm also brought about the same changes in the CV of **ZnTMP-Ph$_2$-PD** as observed for **ZnTMP-Ph-PD** (1.0 equiv. with $E_{1/2}$ of +0.56, +0.80, and +1.14 V; 2.0 equiv. with $E_{1/2}$ of +0.56, +0.62, and +1.24 V).

A comparison of the half-wave potentials observed in the CVs of **PD**, **ZnTMP**, **ZnTMP-PD**, **ZnTMP-Ph-PD**, and **ZnTMP-Ph$_2$-PD** and the changes therein upon HIm titration allows us to identify the nature of the electrochemical reactions occurring in **ZnTMP-Ph-PD** and **ZnTMP-Ph$_2$-PD**.[17] The three reversible redox couples in the CVs of **ZnTMP-Ph-PD**, and **ZnTMP-Ph$_2$-PD** correspond to the loss of one electron on the **PD** moiety ([**ZnP-PD**]$^{+\bullet}$), the following loss of one electron on zinc porphyrin moieties ([**ZnP-PD**]$^{2+}$), and the overlap of

Table 1 Oxidation potentials of **PD**, **ZnTMP**, **ZnTMP-PD**, **ZnTMP-Ph-PD**, and **ZnTMP-Ph$_2$-PD** in the absence or presence of HIm

| | 0.00 equiv. HIm | | | 1.00 equiv. HIm | | | 2.00 equiv. HIm | | |
|---|---|---|---|---|---|---|---|---|---|
| | $E_{ox1}$/V | $E_{ox2}$/V | $E_{ox3}$/V | $E_{ox1}$/V | $E_{ox2}$/V | $E_{ox3}$/V | $E_{ox1}$/V | $E_{ox2}$/V | $E_{ox3}$/V |
| **PD** | +0.59 | +1.01 | | +0.62[a] | | | | | |
| **ZnTMP** | +0.79 | +1.11 | | +0.60 | +1.21 | | | | |
| **ZnTMP-PD** | +0.58 | +0.81 | +1.13[a] | +0.57 | +0.70 | +1.21 | +0.57 | +0.70 | +1.21 |
| **ZnTMP-Ph-PD** | +0.56 | +0.82 | +1.12[a] | +0.56[a] | +0.82 | +1.14 | +0.56[a] | +0.61 | +1.21 |
| **ZnTMP-Ph$_2$-PD** | +0.56 | +0.80 | +1.10[a] | +0.56[a] | +0.80 | +1.14 | +0.56[a] | +0.62 | +1.24 |

[a] Two-electron transfer involved in a redox couple.

respective loss of one electron on both zinc porphyrins and the **PD** moiety ([**ZnP-PD**]$^{4+}$), respectively. The oxidation potentials of all species in various oxidation states are shown in Table 1.

### Spectroelectrochemistry

The variations in the absorption spectra of **ZnTMP-Ph-PD** as a function of the applied potentials ($E_{appl.}$) were investigated by the OTTLE spectroelectrochemical method. With an increase in the applied potential from −0.10 to +0.61 V (Fig. 4(A)), the absorption peak of **ZnTMP-Ph-PD** shows a decrease in the intensities at 316, 322 and 422 nm, in addition to the appearance of a new broad band (600–1000 nm) which can be attributed to the absorption by **PD**$^{+\bullet}$ (Fig. S2, ESI†). Notice that the slight decrease observed in the intensity of the Soret band (422 nm) is indicative of the delocalization of the electron cloud from zinc porphyrin to **PD**$^{+\bullet}$. When the applied potential is further increased from +0.70 to +0.94 V (Fig. 4(B)), the peaks at 422 and 550 nm gradually disappear, while the broad band (500–700 nm) corresponding to the absorption by **ZnTMP**$^{+\bullet}$ grows in intensity (Fig. S3, ESI†). Therefore, we could attribute the second oxidation to the zinc porphyrin. To observe the ligand transfer behaviour of the modified zinc porphyrins, we added 0.75 equivalent of HIm to the zinc porphyrin solution. The observed spectra then results from the mixture of two species, *i.e.* **ZnTMP-Ph-PD** ($\lambda_{Soret}$ = 422 nm) and **(HIm)-ZnTMP-Ph-PD** (shoulder band at 432 nm) (Fig. S4, ESI†). In the potential range from −0.10 to +0.53 V (Fig. 5(A)), there is a decrease in the intensities at 316 and 322 nm along with the formation of a broad band (600–1000 nm). These trends observed in the spectra of the complex are the same as those observed in the absence of HIm, but for the disappearance of band at 432 nm which is the evidence for the **(HIm)-ZnTMP-Ph-PD** to **ZnTMP-Ph-(PD$^{+\bullet}$)(HIm)** transition (enlarged inset in Fig. 5(A)). The likely reason for the observed transfer of the ligand from one moiety to other is the post-oxidation change in the relative binding constants. The binding constant for HIm with an oxidized **PD** is larger than that for HIm with the neutral zinc porphyrin. Nevertheless, from our previous studies with **ZnTMP-PD** (Fig. S5, ESI†),[12] the transition between four and five coordinated zinc porphyrin was unclear at the increasing absorption spectra of four coordinated zinc porphyrin ($\lambda_{Soret}$ = 422 nm). In the recovery experiment (after the initial application of +0.53 V, the potential was reverted to

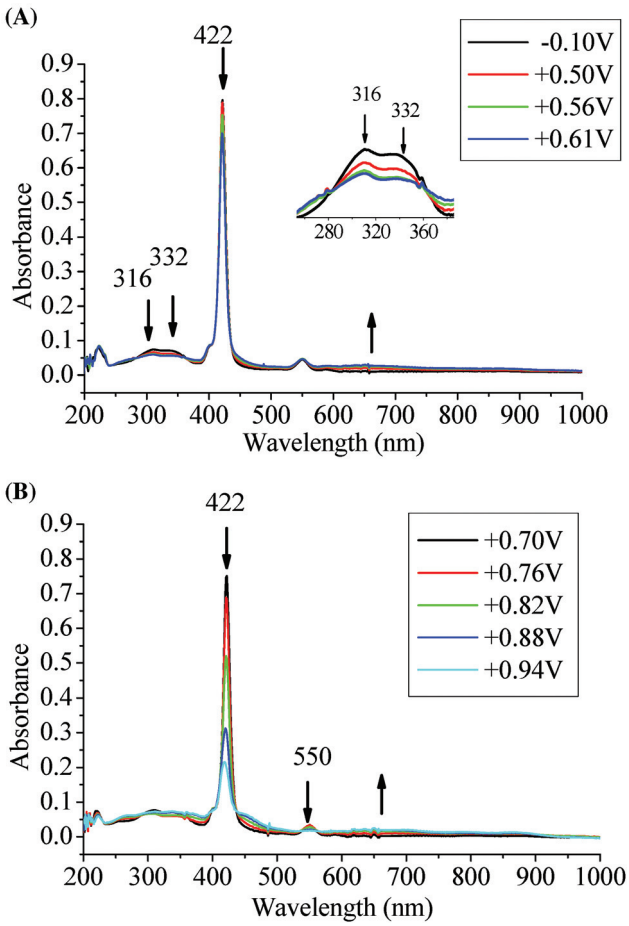


Fig. 4 Potential dependent spectral changes of 4.0 × 10$^{-5}$ M **ZnTMP-Ph-PD** in the absence of HIm in $CH_2Cl_2$ containing 0.1 M TBAP.

0.00 V), the recovery of **ZnTMP-Ph-PD** (53%) is lower than that of **ZnTMP-PD** (73%), showing irreversibility. The absence of protection at the *meso* position leads to easier decomposition of the oxidized porphyrin and results in a decrease of intensity in each absorption band.[18] Therefore, we propose that the decomposition of zinc porphyrin along with the longer bridge is the likely reason for the ambiguous spectral change representing the transition of HIm from **(HIm)ZnTMP-Ph-PD** to **ZnTMP-Ph-(PD$^{+\bullet}$)(HIm)**. A potential range of +0.56 to +0.68 V (Fig. 5(B)) is not typically positive enough to oxidize the zinc porphyrin moiety, however, the observed slight decrease in the

 

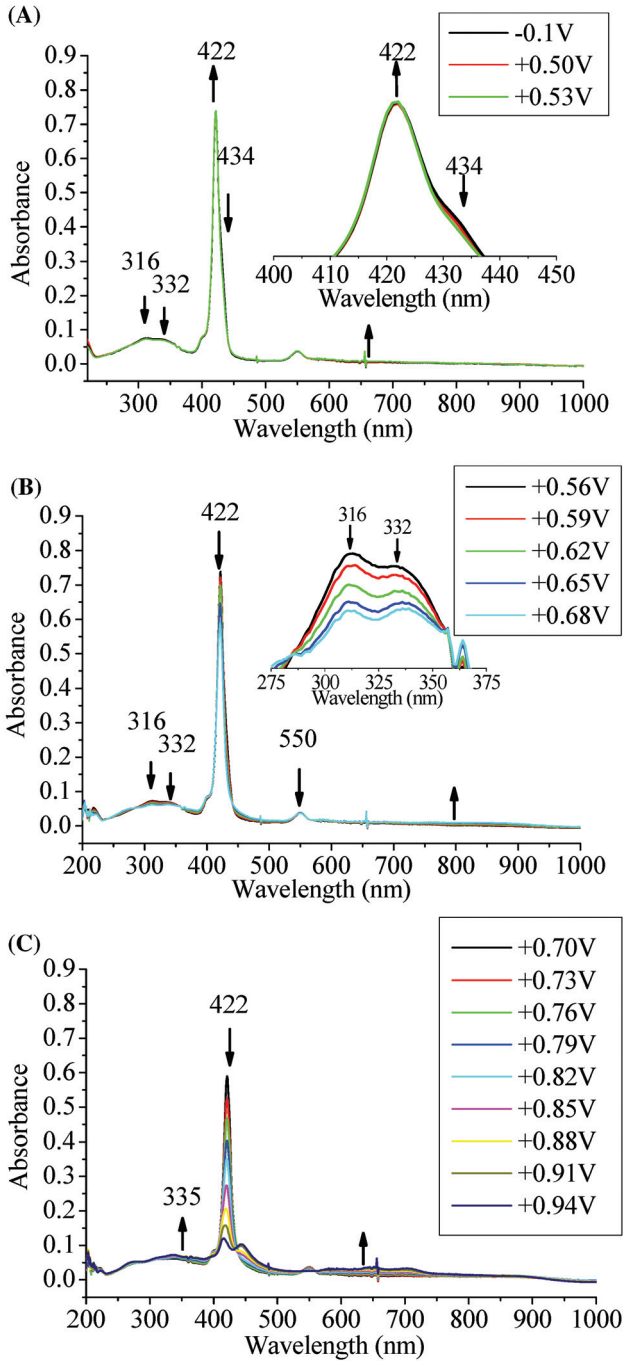


**Fig. 5** Potential dependent spectral changes of $4.0 \times 10^{-5}$ M **ZnTMP-Ph-PD** in the presence of 0.75 equivalents HIm in $CH_2Cl_2$ containing 0.1 M TBAP.

intensity of the peak at 422 nm in the absorption spectra is a characteristic of oxidized zinc porphyrin (Fig. S3, ESI†). It indicates a likelihood of interaction between two redox centres that is caused by the delocalization of the electron density from the zinc porphyrin ring to $\mathbf{PD}^{+\bullet}$. With the increase in applied potential from +0.70 to +0.94 V (Fig. 5(C)), the absorption at 422 nm gradually disappears, while a broad band (500–700 nm) grows, indicating the formation of cation radical of zinc porphyrin, $\mathbf{ZnTMP}^{+\bullet}$**-Ph-**$\mathbf{PD}^{+\bullet}$.

In the case of **ZnTMP-Ph$_2$-PD**, the patterns of change in spectra are similar to those of **ZnTMP-Ph-PD** (Fig. S6 and S7, ESI†). However, a more severe decomposition of oxidized zinc porphyrin competes with the transition of **ZnTMP-Ph$_2$-PD** to **(HIm)ZnTMP-Ph$_2$-PD** (recovery of cation radical is ~40%), and presents difficulties in the spectral analysis (enlarged picture in Fig. S7†). On the basis of the decrease in the intensity in the absorption spectra at 422 nm after the transition of **ZnTMP-Ph$_2$-PD** to **(HIm)ZnTMP-Ph$_2$-PD**, we infer that the decomposition continued at the applied oxidative state. These data present spectral evidence for the transfer of the HIm ligand from zinc porphyrin to the **PD** moiety, even when the distance between the two redox centres has changed.

### Binding constants between zinc porphyrin and HIm

To gain further insights into the transfer of HIm between **PD** and zinc porphyrin moieties, the binding constants of HIm with zinc porphyrin in various oxidation states were further surveyed. To determine the binding constants of the neutral and cation radical states of the zinc porphyrin moiety, we independently titrated **ZnTMP-Ph-PD** and **ZnTMP-Ph$_2$-PD** with HIm and monitored the resulting UV-Vis spectra. With increasing concentration of HIm the absorption band (Q band) of **ZnTMP-Ph-PD** decreases at 550 nm, and increases at 567 and 607 nm. Furthermore, three well-defined isosbestic points appear at 558, 586, and 593 nm, indicating a conversion of **ZnTMP-Ph-PD** to **(HIm)ZnTMP-Ph-PD** (Fig. S8 ESI†).[19] The absorption spectra of **ZnTMP-Ph$_2$-PD** exhibit a similar pattern (Fig. S9, ESI†). The reported binding constant of **ZnTMP-Ph-PD** with HIm is $4.84 \times 10^4$ $M^{-1}$, and that of **ZnTMP-Ph$_2$-PD** is $1.87 \times 10^5$ $M^{-1}$.[20] In contrast to **ZnTMP-PD**,[17] the order of the binding constants are **ZnTMP-Ph$_2$-PD** > **ZnTMP-Ph-PD** > **ZnTMP-PD**. The binding constants between HIm and the oxidized zinc porphyrin moiety were also calculated as described previously based on the potential shift of CVs (Table 1).[21] The binding constants of $[\mathbf{ZnTMP\text{-}Ph\text{-}PD}]^{+\bullet}$ and $[\mathbf{ZnTMP\text{-}Ph_2\text{-}PD}]^{+\bullet}$ are $2.60 \times 10^7$ $M^{-1}$ and $1.00 \times 10^8$ $M^{-1}$, respectively (Table 2). The details of calculations for determining the binding constants of neutral and cation radical states of the zinc porphyrin moiety are shown in page S11, ESI† (Scheme 1).

**Table 2** Binding constants for HIm with **PD**, **ZnTMP**, **ZnTMP-PD**, **ZnTMP-Ph-PD**, and **ZnTMP-Ph$_2$-PD** in various oxidation states

| Molecule | Binding constant ($K$) ($M^{-1}$) | Reference |
|---|---|---|
| $\mathbf{PD}^{+\bullet}$ | 4500 | [a] |
| $\mathbf{PD}^{2+}$ | $2.76 \times 10^{12}$ | [a] |
| **ZnTMP** | $1.92 \times 10^4$ | 17 |
| $\mathbf{ZnTMP}^{+\bullet}$ | $5.13 \times 10^7$ | 17 |
| $\mathbf{ZnTMP}^{2+}$ | $9.19 \times 10^1$ | 17 |
| **ZnTMP-PD** | $2.32 \times 10^4$ | 12 |
| $\mathbf{ZnTMP\text{-}PD}^{+\bullet}$ | $1.24 \times 10^7$ | 12 |
| **ZnTMP-Ph-PD** | $4.84 \times 10^4$ | [a] |
| $\mathbf{ZnTMP\text{-}Ph\text{-}PD}^{+\bullet}$ | $2.60 \times 10^7$ | [a] |
| **ZnTMP-Ph$_2$-PD** | $1.87 \times 10^5$ | [a] |
| $\mathbf{ZnTMP\text{-}Ph_2\text{-}PD}^{+\bullet}$ | $1.00 \times 10^8$ | [a] |

[a] This work.

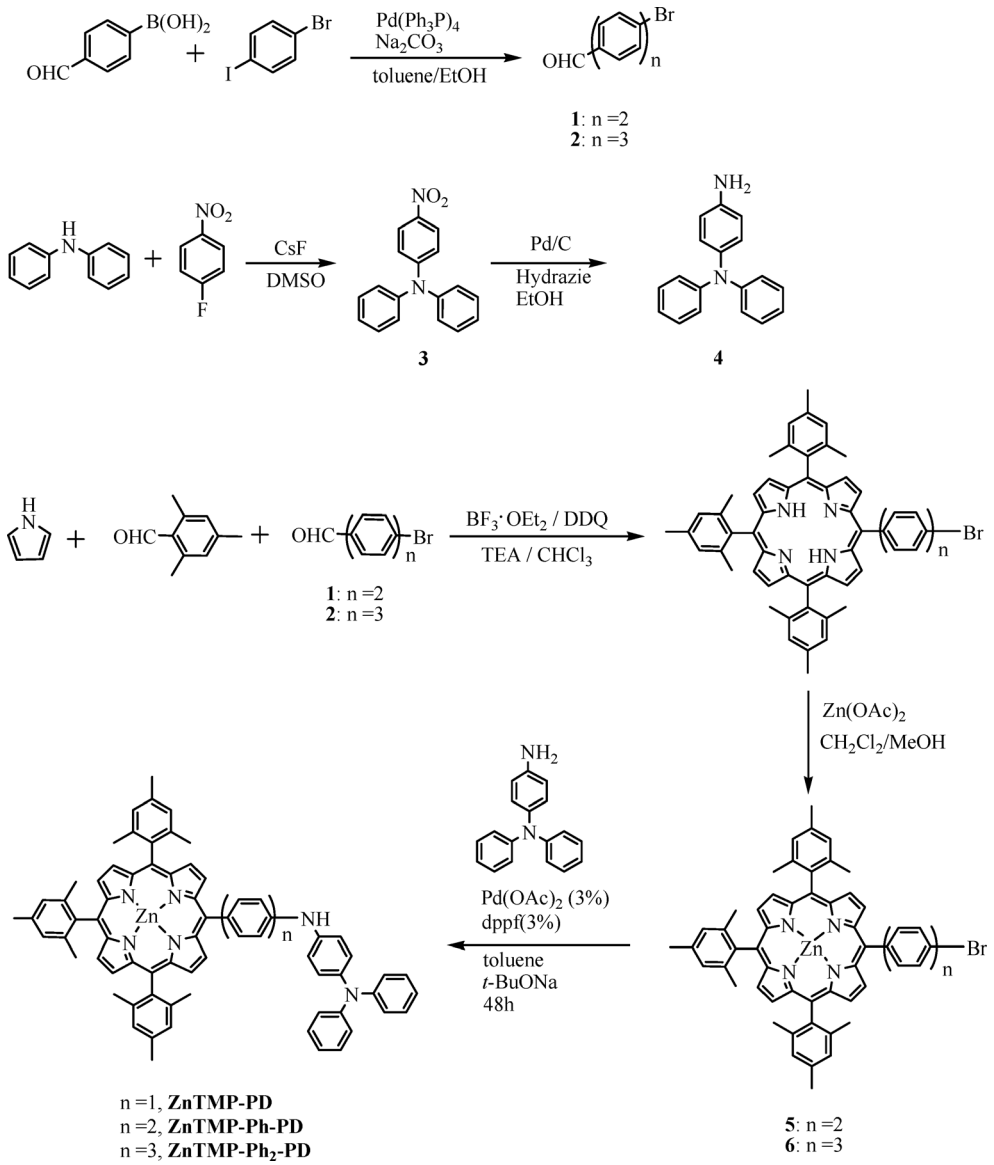


**Scheme 1** Synthesis of **ZnTMP-(Ph)$_n$-PD**.

As for the binding constant of HIm with oxidized **PD**, the best way to obtain quantitative information on electrochemically induced binding systems is the use of digital simulations to obtain a fit for the experimentally acquired voltammograms.[22–26] The reaction mechanism consisting of only electron transfers and hydrogen bonding equilibria is represented by the six-membered square scheme in Scheme 2. DigiSim (v 3.03) was used to carry out the digital simulations of experimental CVs. The values for oxidation potentials of **PD** ($E_1^{ox}$ and $E_2^{ox}$), the diffusion coefficient ($D$), and the uncompensated resistance ($R_u$) were determined first by fitting the CVs of **PD** recorded in the absence of imidazole. The magnitude of current was fitted by adjusting the value of $D$. For all uncomplexed **PD**, $D$ is assumed to have the same value of $1.0 \times 10^{-5}$ cm$^2$ s$^{-1}$. The peak-to-peak separation was fitted by adjusting the values of $D$ and $R_u$. The value of $R_u$ resulting from the fit was 290 Ω. The determined $E_1^{ox'}$, $E_2^{ox'}$, $D$, and $R_u$ were then used to fit the complete sets of CVs recorded during titration. The value of $K_1$ depends both on the shift in $E_1^{ox}$ and the binding constant associated with the neutral state, while $K_2$ is related

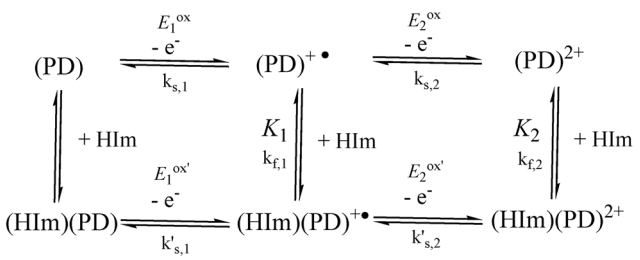


**Scheme 2** Equilibria in the square reaction mechanism for the redox-dependent binding of HIm to **PD**.

 

Table 3 Parameters for the simulation of the CV for the PD/HIm system[a]

| | Electrochemical reactions | $E^0$ | $k_s$ (cm $s^{-1}$) |
|---|---|---|---|
| $E_1^{ox}$ | $(PD)^+ + e = (PD)$ | 0.61 V | 1 |
| $E_2^{ox}$ | $(PD)^{2+} + e = (PD)^+$ | 1.03 V | 0.03 |
| $E_1^{ox'}$ | $(PD)(HIm)^+ + e = (PD)(HIm)$ | 0.61 V | 10 |
| $E_2^{ox'}$ | $(PD)(HIm)^{2+} + e = (PD)(HIm)^+$ | 0.51 V | 0.005 |
| | Chemical reactions | $K$ | $k_f$ |
| $K_1$ | $(PD)^+ + (HIm) = (PD)(HIm)^+$ | 4500 $M^{-1}$ | $1.0 \times 10^8$ $M^{-1}$ $s^{-1}$ |
| $K_2$ | $(PD)^{2+} + (HIm) = (PD)(HIm)^{2+}$ | $2.76 \times 10^{12}$ $M^{-1}$ | $1.0 \times 10^{10}$ $M^{-1}$ $s^{-1}$ |

[a] Diffusion coefficient ($D$) for **PD**, $PD^+$, $PD^{2+}$, (**PD**)(HIm), $(PD)(HIm)^+$, and $(PD)(HIm)^{2+}$ were set to be $1.0 \times 10^{-5}$ $cm^2$ $s^{-1}$; $D$ for (HIm) = $5.0 \times 10^{-5}$ $cm^2$ $s^{-1}$; $R_u$ = 290 Ω; $A$ = 0.07 $cm^2$; all transfer coefficients ($\alpha$) = 0.5; scan rate = 0.1 V $s^{-1}$.

to the change in $E_2^{ox}$. The determination of the $K_1$ is particularly important because its value largely determines the behaviour in the second oxidation, which would exhibit two different types, two resolved waves or shifted waves in the electrochemically induced ligand binding system.[22] Based on our previous studies with electrochemically induced hydrogen bonding between oxidized **PD** and pyridines ($pK_a$ = 0.67–7.48), reasonable starting values for $K_1$ could be assumed for the simulations.[17] Since the $pK_a$ of HIm is 6.92, the binding constant of cation radical, $PD^{+\bullet}$ with HIm ($K_1$) was estimated to be 4500 $M^{-1}$ and the one of dication, $PD^{2+}$ and HIm ($K_2$) was calculated to be $2.76 \times 10^{12}$ $M^{-1}$. In addition, for the shift in $E_{1/2}$ to be observed, the forward rate of hydrogen bond formation should be fast. Therefore, with values for kinetic constants $k_{f,1}$ and $k_{f,2}$ in the $10^8$–$10^{10}$ $M^{-1}$ $s^{-1}$ range, we could obtain the best fit for the CVs as shown in Fig. 1(B). Other parameters are listed in Table 3.

The binding constants of **PD**, **ZnTMP**, **ZnTMP-PD**, **ZnTMP-Ph-PD** and **ZnTMP-Ph$_2$-PD** in various states of oxidation (Table 2) explain the ligand transfer behaviour of this electrochemically controlled system. In the initial neutral state, HIm ligates to the centre of the zinc porphyrin moiety ($K$ = $10^4$–$10^5$ $M^{-1}$). After the electrode potential induced oxidation of the **PD** moiety, the binding site of HIm shifts to the **PD** moiety (since $K$ = ~$10^{12}$ $M^{-1}$). As the oxidation potential becomes more positive, the zinc porphyrin is further oxidized. However, with a binding constant in the $10^7$–$10^8$ $M^{-1}$ range for HIm with electron deficient zinc porphyrins, the reversal of the HIm ligand from the oxidized **PD** moiety to the oxidized zinc porphyrin is unlikely and forbidden. Scheme 3 shows the oxidation dependent changes in ligation of HIm in the **PD**-substituted zinc porphyrin system. This ligand transfer system, then, is an electrochemically controlled switch rather than a shuttle.

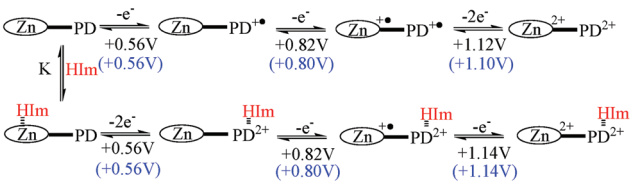


Scheme 3 Electrochemically controlled ligation of HIm with **ZnTMP-Ph-PD** (black letters) and **ZnTMP-Ph$_2$-PD** (blue letters).

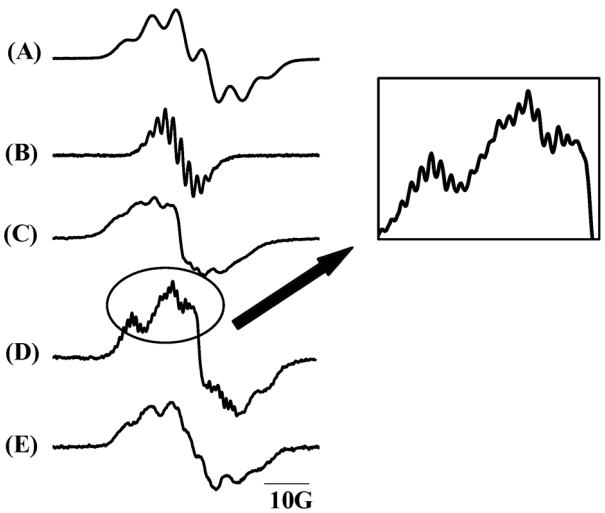


Fig. 6 EPR spectra of (A) $PD^{+\bullet}$, (B) $ZnTMP^{+\bullet}$, (C) $ZnTMP\text{-}PD^{+\bullet}$, (D) $ZnTMP\text{-}Ph\text{-}PD^{+\bullet}$, and (E) $ZnTMP\text{-}Ph_2\text{-}PD^{+\bullet}$ at 298 K.

### EPR studies on electron transfer in modified zinc porphyrins

To observe the electronic interactions between zinc porphyrin and the **PD** moiety, cation radicals $PD^{+\bullet}$, $ZnTMP^{+\bullet}$, $ZnTMP\text{-}PD^{+\bullet}$, $ZnTMP\text{-}Ph\text{-}PD^{+\bullet}$, and $ZnTMP\text{-}Ph_2\text{-}PD^{+\bullet}$ were generated *in situ* at 298 K in $CH_2Cl_2$ and were found to be stable at room temperature. Those systems were separated into two portions, **ZnTMP** and **PD**. The six-line spectrum of $PD^{+\bullet}$ centred at $g$ = 2.0030 is different from the isoelectronic $N2^{+\bullet}$ with a five-line spectrum because a phenyl group is replaced by a proton with hyperfine coupling interaction of ~4.6 G, contributing two nitrogen ions with ~5.7 G for each, as shown in Fig. 6(A) (Fig. S10, ESI†). The EPR spectrum of $ZnTMP^{+\bullet}$ (Fig. 6(B)) is a representative of the typical pattern observed for **ZnTMP** porphyrin macrocycles oxidized at the $a_{2u}$ orbital with $g$ = 2.0030. In the spectrum of $ZnTMP\text{-}Ph\text{-}PD^{+\bullet}$, the splitting due to hyperfine coupling ascribed to $ZnTMP^{+\bullet}$ is found to be superimposed on the primary pattern of $PD^{+\bullet}$ (Fig. 6(D) and the enlarged inset). This well-resolved spectrum demonstrates

that the radical is delocalized between the porphyrin ring and the **PD** moiety. In contrast, for the phenyl-linker lacking **ZnTMP-PD**$^{+\bullet}$, the EPR splitting appears to be similar to that obtained from a mixture of **ZnTMP**$^{+\bullet}$ and **PD**$^{+\bullet}$. In contrast, when the linker is composed of two phenyl groups, the EPR spectrum is similar to that of **ZnTMP-Ph-PD**$^{+\bullet}$, but with smaller hyperfine couplings (Fig. 6(C) and (E)). The EPR spectrum of **ZnTMP-PD**$^{+\bullet}$ has an obscure cleavage, and a broad line width which is similar to the pattern observed for **PD**$^{+\bullet}$. The interaction between the two redox centres is proportional to the hyperfine coupling constants. The larger hyperfine coupling constant of **ZnTMP**$^{+\bullet}$**-PD**$^{+\bullet}$ was not split easily on the shape. It seems like a merger of both hyperfine couplings from zinc porphyrin and the **PD** moiety occurs. In contrast with the EPR spectrum of **ZnTMP**$^{+\bullet}$**-Ph$_2$-PD**$^{+\bullet}$ had the same broad line width, but the cleavage was easy to distinguish because of the smaller hyperfine coupling constant.

## Conclusions

We report here that both **ZnTMP-Ph-PD** and **ZnTMP-Ph$_2$-PD** exhibit an ability to switch the binding sites for the ligand HIm. In the neutral state, HIm is coordinated as an axial ligand to form a five-coordinated zinc porphyrin. In the presence of HIm, the **PD** moiety loses two electrons on oxidation due to the electrochemically induced formation of hydrogen bond. Since the affinity of HIm for **PD**$^{2+}$ is greater than its affinity for the neutral zinc porphyrin, HIm is repositioned to bind with **PD**$^{2+}$. Further application of a more positive potential leads to the formation of a cation radical of the zinc porphyrin moiety; however, the binding constant of HIm with the oxidized zinc porphyrin is smaller than that for HIm and the **PD**$^{2+}$ moiety. Therefore, the shuttling behaviour could not be seen in this system. A switch from **PD** back to the zinc porphyrin moiety could, however, be observed on returning to the neutral state. Furthermore, the length of the covalent bridge affects the binding constant of the five-coordinated zinc porphyrin with the following trend in the magnitude: **ZnTMP-Ph$_2$-PD** > **ZnTMP-Ph-PD** > **ZnTMP-PD**.

For studies related to electron transfer behaviour, it was observed that the length of the covalent bridge that links the two moieties critically influences the delocalization of electrons from the **PD** to the **ZnTMP** moiety. A shorter bridge is beneficial for better electron transfer. It is likely that the electron density of each moiety can be controlled by varying the degree of delocalization of the bridge in this progressive switch (Chart 2). The EPR spectra further substantiated the proposed model for this phenomenon.

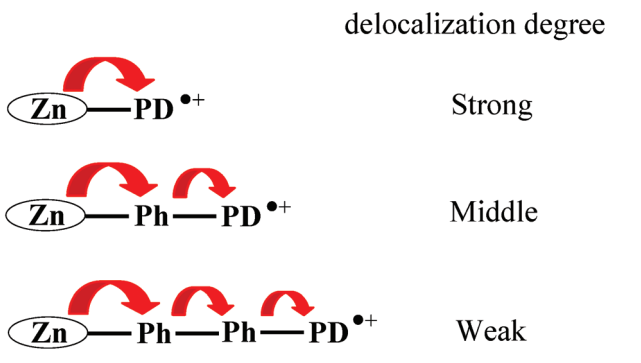


Chart 2 Degree of delocalization in the ZnTMP-bridge-PD system.

## Acknowledgements

The authors thank the National Science Council of Taiwan, Republic of China, for support of this work.

## Notes and references

1 J. T. Groves, K. Shalyaev and J. Lee, in *The Porphyrin Handbook*, ed. K. M. Kadish, K. M. Smith, R. Guilard, Academic Press, New York, 2000, vol. 4, p. 17.
2 N. A. Stephenson and A. T. Bell, *J. Mol. Catal. A: Chem.*, 2007, **272**, 108.
3 C. Monnereau, J. Gomez, E. Blart and F. Odobel, *Inorg. Chem.*, 2005, **44**, 4806.
4 A. Kira, T. Umeyama, Y. Matano, K. Yoshida, S. Isoda, J. K. Park, D. Kim and H. Imahori, *J. Am. Chem. Soc.*, 2009, **131**, 3198.
5 C.-Y. Liu and A. J. Bard, *Acc. Chem. Res.*, 1999, **32**, 235–245.
6 F. Fungo, L. Otero, C. D. Borsarelli, E. N. Durantini, J. J. Silber and L. Sereno, *J. Phys. Chem. B*, 2002, **106**, 4070.
7 M. Gervaldo, F. Fungo, E. N. Durantini, J. J. Silber, L. Sereno and L. Otero, *J. Phys. Chem. B*, 2005, **109**, 20953.
8 C. M. Drain, A. Varotto and I. Radivojevic, *Chem. Rev.*, 2009, **109**, 1630.
9 S. F. Miller and G. T. Babcock, *Chem. Rev.*, 1996, **96**, 2889.
10 G. T. Babcock and M. Wikstrom, *Nature*, 1992, **356**, 301.
11 J. P. Abrahams, A. G. W. Leslie, R. Lutter and J. E. Walker, *Nature*, 1994, **370**, 621.
12 K. Y. Chiu and Y. O. Su, *Chem. Commun.*, 2009, 2884.
13 J. Bu, N. D. Lilienthal, J. E. Woods, C. E. Nohrden, K. T. Hoang, D. Truong and D. K. Smith, *J. Am. Chem. Soc.*, 2005, **127**, 6423.
14 Y. Ge, R. R. Lilienthal and D. K. Smith, *J. Am. Chem. Soc.*, 1996, **118**, 3976.
15 Y. Hirao, A. Ito and K. Tanaka, *J. Phys. Chem. A*, 2007, **111**, 2951.
16 D. Simoni, G. Giannini, M. Roberti, R. Rondanin, R. Baruchello, M. Rossi, G. Grisolia, F. P. Invidiata, S. Aiello, S. Marino, S. Cavallini, A. Siniscalchi, N. Gebbia, L. Crosta, S. Grimaudo, V. Abbadessa, A. D. Cristina and M. Tolomeo, *J. Med. Chem.*, 2005, **48**, 4293.
17 Y. C. Chung, Y. J. Tu, S. H. Lu, W. C. Hsu, K. Y. Chiu and Y. O. Su, *Org. Lett.*, 2011, **13**, 2826.

18 (*a*) R. Guilard, N. Jagerovic, A. Tabard, C. Naillon and K. M. Kadish, *J. Chem. Soc., Dalton Trans.*, 1992, 1957; (*b*) Y. O. Su, D. Kim and T. G. Spiro, *Electroanal. Chem.*, 1987, **234**, 145; (*c*) C. K. Chang, G. Aviles and N. Bag, *J. Am. Chem. Soc.*, 1994, **116**, 12127.
19 C. L. Lin, M. Y. Fang and S. H. Cheng, *J. Electroanal. Chem.*, 2002, **531**, 155.
20 G. S. Marbury, C. Brewer and G. Brewer, *J. Chem. Soc., Dalton Trans.*, 1991, 1377.
21 K. M. Kadish, L. R. Shiue, R. K. Rhodes and L. A. Bottomley, *Inorg. Chem.*, 1981, **20**, 1274.
22 S. R. Miller, D. A. Gustowski, Z. H. Chen, G. W. Gokel, L. Echegoyen and A. E. Kaifer, *Anal. Chem.*, 1988, **60**, 2021.
23 D. H. Evans, *Chem. Rev.*, 2008, **108**, 2113.
24 J. Bu, N. D. Lilienthal, J. E. Woods, C. E. Nohrden, K. T. Hoang, D. Truong and D. K. Smith, *J. Am. Chem. Soc.*, 2005, **127**, 6423.
25 C. C. Leonor, S. L. Martin and D. K. Smith, *J. Org. Chem.*, 2005, **70**, 10817.
26 H. C. Cheng, K. Y. Chiu, Y. J. Tu, T. F. Yang and Y. O. Su, *Org. Lett.*, 2013, **15**, 3868.